High-spin structure of ^{134}Xe

A. Vogt,[1,*] B. Birkenbach,[1] P. Reiter,[1] A. Blazhev,[1] M. Siciliano,[2,3] J. J. Valiente-Dobón,[3] C. Wheldon,[4] D. Bazzacco,[5]
M. Bowry,[6] A. Bracco,[7] B. Bruyneel,[8] R. S. Chakrawarthy,[9] R. Chapman,[10] D. Cline,[11] L. Corradi,[3] F. C. L. Crespi,[7]
M. Cromaz,[12] G. de Angelis,[3] J. Eberth,[1] P. Fallon,[12] E. Farnea,[5,†] E. Fioretto,[3] S. J. Freeman,[9] A. Gadea,[13] K. Geibel,[1]
W. Gelletly,[6] A. Gengelbach,[14] A. Giaz,[7] A. Görgen,[15,16,12] A. Gottardo,[3] A. B. Hayes,[11] H. Hess,[1] H. Hua,[11] P. R. John,[2,5]
J. Jolie,[1] A. Jungclaus,[17] W. Korten,[16] I. Y. Lee,[12] S. Leoni,[7] X. Liang,[18] S. Lunardi,[2,5] A. O. Macchiavelli,[12] R. Menegazzo,[5]
D. Mengoni,[18,2,5] C. Michelagnoli,[2,5,‡] T. Mijatović,[19] G. Montagnoli,[2,5] D. Montanari,[2,5,§] D. Napoli,[3] C. J. Pearson,[6,‖]
L. Pellegri,[7] Zs. Podolyák,[6] G. Pollarolo,[20] A. Pullia,[7] F. Radeck,[1] F. Recchia,[2,5] P. H. Regan,[6,21] E. Şahin,[3,¶] F. Scarlassara,[2,5]
G. Sletten,[22] J. F. Smith,[18] P.-A. Söderström,[14,#] A. M. Stefanini,[3] T. Steinbach,[1] O. Stezowski,[23] S. Szilner,[19] B. Szpak,[24]
R. Teng,[11] C. Ur,[5] V. Vandone,[7] D. Ward,[12] D. D. Warner,[25,†] A. Wiens,[1] and C. Y. Wu[11,**]

[1]*Institut für Kernphysik, Universität zu Köln, D-50937 Köln, Germany*
[2]*Dipartimento di Fisica e Astronomia, Università di Padova, I-35131 Padova, Italy*
[3]*Istituto Nazionale di Fisica Nucleare, Laboratori Nazionali di Legnaro, I-35020 Legnaro, Italy*
[4]*School of Physics and Astronomy, University of Birmingham, Birmingham B15 2TT, United Kingdom*
[5]*Istituto Nazionale di Fisica Nucleare, Sezione di Padova, I-35131 Padova, Italy*
[6]*Department of Physics, University of Surrey, Guildford, Surrey GU2 7XH, United Kingdom*
[7]*Dipartimento di Fisica, Università di Milano and INFN Sezione di Milano, I-20133 Milano, Italy*
[8]*CEA Saclay, Service de Physique Nucleaire, F-91191 Gif-sur-Yvette, France*
[9]*Department of Physics and Astronomy, Schuster Laboratory, University of Manchester, Manchester M13 9PL, United Kingdom*
[10]*SUPA, School of Engineering and Computing, University of the West of Scotland, Paisley PA1 2BE, United Kingdom*
[11]*Department of Physics, University of Rochester, Rochester, New York 14627, USA*
[12]*Lawrence Berkeley National Laboratory, Berkeley, California 94720, USA*
[13]*Instituto de Física Corpuscular, CSIC-Universidad de Valencia, E-46071 Valencia, Spain*
[14]*Department of Physics and Astronomy, Uppsala University, SE-75121 Uppsala, Sweden*
[15]*Department of Physics, University of Oslo, Post Office Box 1048 Blindern, N-0316 Oslo, Norway*
[16]*Institut de Recherche sur les lois Fondamentales de l'Univers (IRFU), CEA/DSM, Centre CEA de Saclay,*
F-91191 Gif-sur-Yvette Cedex, France
[17]*Instituto de Estructura de la Materia, CSIC, Madrid, E-28006 Madrid, Spain*
[18]*Nuclear Physics Research Group, University of the West of Scotland, High Street, Paisley PA1 2BE, Scotland, United Kingdom*
[19]*Ruđer Bošković Institute, HR-10 002 Zagreb, Croatia*
[20]*Dipartimento di Fisica Teorica dell'Università di Torino and INFN, I-10125 Torino, Italy*
[21]*Radioactivity Group, National Physical Laboratory, Teddington, Middlesex, TW11 0LW, United Kingdom*
[22]*Niels Bohr Institute, University of Copenhagen, Blegdamsvej 17, 2100 Copenhagen, Denmark*
[23]*Université de Lyon, Université Lyon-1, CNRS/IN2P3, UMR5822, IPNL, F-69622 Villeurbanne Cedex, France*
[24]*Henryk Niewodniczański Institute of Nuclear Physics PAN, PL-31342 Kraków, Poland*
[25]*CCLRC Daresbury Laboratory, Warrington WA4 4AD, United Kingdom*

Detailed spectroscopic information on the $N \sim 82$ nuclei is necessary to benchmark shell-model calculations in the region. The nuclear structure above long-lived isomers in ^{134}Xe is investigated after multinucleon transfer (MNT) and actinide fission. Xenon-134 was populated as (i) a transfer product in ^{136}Xe $+$ ^{238}U and ^{136}Xe $+$ ^{208}Pb MNT reactions and (ii) as a fission product in the ^{136}Xe $+$ ^{238}U reaction employing the high-resolution Advanced Gamma Tracking Array (AGATA). Trajectory reconstruction has been applied for the complete identification of beamlike transfer products with the magnetic spectrometer PRISMA. The ^{136}Xe $+$ ^{198}Pt MNT reaction was studied with the γ-ray spectrometer GAMMASPHERE in combination with the gas detector array Compact Heavy Ion Counter (CHICO). Several high-spin states in ^{134}Xe on top of the two long-lived isomers are discovered based on $\gamma\gamma$-coincidence relationships and information on the γ-ray angular distributions as well as excitation energies from the total kinetic energy loss and fission fragments. The revised level scheme of ^{134}Xe is extended up to an

---

*Corresponding author: andreas.vogt@ikp.uni-koeln.de

†Deceased.

‡Present address: GANIL, CEA/DSM-CNRS/IN2P3, F-14076, Caen, France.

§Present address: USIAS - Université de Strasbourg, IPHC-CNRS, F-67037 Strasbourg Cedex 2, France.

‖Present address: TRIUMF, 4004 Wesbrook Mall, Vancouver, British Columbia V6T 2A3, Canada.

¶Present address: Department of Physics, University of Oslo, P. O. Box 1048 Blindern, N-0316 Oslo, Norway.

#Present address: RIKEN Nishina Center, Wako, 351-0198 Saitama, Japan.

**Present address: Lawrence Livermore National Laboratory, Livermore, California 94551, USA.

excitation energy of 5.832 MeV with tentative spin-parity assignments up to 16^+. Previous assignments of states above the 7^- isomer are revised. Latest shell-model calculations employing two different effective interactions reproduce the experimental findings and support the new spin and parity assignments.

I. INTRODUCTION

The nuclear structure of high-spin states in the vicinity of the $N = 82$ magic number is of high interest to benchmark nuclear shell-model calculations. Isomeric yrast $I^\pi = 10^+$ states of $\nu h_{11/2}^{-2}$ character have been reported in all the even-mass $N = 80$ isotones ranging from ^{130}Sn to ^{142}Sm [1–8]. Comprehensive shell-model (SM) calculations and detailed predictions for these nuclei are the subject of several recent studies, which are either based on the jj coupled scheme or on the uncoupled m scheme. The jj scheme is adopted by the codes NATHAN [9,10] and NUSHELLX [11]. It has the advantage of yielding shell-model Hamiltonian matrices of relatively small dimensions. On the other hand, these matrices are very dense and have complex algebraic structures. The Xe isotopes with four valence protons and increasing deformation have come within reach of these types of advanced shell-model calculations. With respect to the Sn isotopes, the number of neutron holes is increased and the deformation is driven by the proton-neutron force, which acts efficiently in Xe isotopes. Therefore, the Xe isotopes provide an intriguing and important test case for new shell-model developments. In summary, the following theoretical studies were performed employing pair-truncated shell-model calculations [12], large scale shell-model calculations [13], and shell-model frameworks with the monopole and quadrupole pairing plus quadrupole-quadrupole interaction employed as an effective interaction [14].

This work focuses on the $N = 80$ isotone $^{134}_{54}$Xe, located in the proton midshell between the $Z = 50$ shell closure and the $Z = 64$ subshell one. The data on low-spin states in ^{134}Xe originate from earlier work employing β decay [15–18] and Coulomb excitation [19,20]. The most recent study was performed by Ahn *et al.* [21]. The authors obtained absolute $E2$ and $M1$ transition strengths in ^{134}Xe in an inverse kinematics ^{12}C(^{134}Xe, ^{134}Xe$'$) Coulomb excitation experiment employing the GAMMASPHERE array at the superconducting Argonne Tandem Linac Accelerator System (ATLAS) accelerator. The 1100-keV transition was validated to connect the mixed-symmetry 2_3^+ state with the first excited 2_1^+ state.

Excited states above the yrast $I^\pi = 10^+$ isomeric state were identified only recently. The first relevant results were obtained by Fotiades *et al.* [22], measuring a variety of fusion-fission fragments from the ^{226}Th compound nucleus via triple-γ coincidences using the GAMMASPHERE array at the Lawrence Berkeley National Laboratory (LBNL) in 2007. A cascade based on a 1323-keV γ-ray transition was attributed to ^{135}Xe by means of $\gamma\gamma$ coincidences. However, the same sequence of γ rays with energies of 218, 320, and 1323 keV was found in an experiment by Shrivastava *et al.* [23] in 2009. The reaction products of the fusion-fission reaction ^{12}C(^{238}U, ^{134}Xe)Ru were unambiguously identified with the magnetic mass spectrometer VAriable MOde high acceptance Spec-

trometer (VAMOS). γ-ray decays of excited states in ^{134}Xe were measured with two EXOGAM Compton-suppressed segmented clover detectors at the Grand Accélérateur National d'Ions Lourds. The γ rays with energies of 218, 320, and 1323 keV and additional lines at 612 and 1100 keV were observed in coincidence with ^{134}Xe, correcting the assignment by Fotiades *et al.* Shrivastava *et al.* argue that all observed lines feed the long-lived 10^+ [$T_{1/2} = 5(1)\mu$s] [2] and 7^- [$T_{1/2} = 290(17)$ ms] isomers [24]. The authors claim that the transitions below those isomeric states are not observed, although a clear indication for the 847-keV $2_1^+ \rightarrow 0^+$ transition below the isomeric states is visible in the corresponding γ-ray spectrum. The observed γ-ray transitions were ordered into cascades above the aforementioned isomers. Due to low statistics, no $\gamma\gamma$ coincidences were analyzed [23]. The placement of the excited states and spin/parity assignments were guided and suggested by the results of a large-scale shell model (LSSM) calculation.

These findings, together with recent theoretical advances, motivated a refined investigation of the nuclear structure in ^{134}Xe, especially regarding high-spin states above the two long-lived isomers. In this article, we report and discuss new results for the nucleus ^{134}Xe obtained in three different experiments, which are based on direct identification of ^{134}Xe and coincident prompt γ-ray spectroscopy. The combination of the high-resolution position-sensitive Advanced Gamma Tracking Array (AGATA) [25] and the PRISMA magnetic mass spectrometer [26–28] was employed to study ^{134}Xe after ^{136}Xe + ^{208}Pb multinucleon transfer (MNT) and ^{136}Xe + ^{238}U MNT and fission reactions, respectively. Further, ^{134}Xe was measured after a ^{136}Xe + ^{198}Pt MNT reaction using the GAMMASPHERE+CHICO setup [29,30] at LBNL.

This paper is organized as follows: the experimental setup, data analysis, and the results of the three experiments are described in Sec. II. A detailed comparison with two modern shell-model calculations is presented in Sec. III, before the paper closes with a summary and conclusions.

II. EXPERIMENTAL PROCEDURE AND RESULTS

A. ^{136}Xe + ^{238}U

In this experiment, the PIAVE+ALPI accelerator complex provided a ^{136}Xe beam with an energy of 1 GeV and a beam current of 2 pnA, impinging onto ^{238}U targets. The ^{238}U targets had thicknesses of 1 and 2 mg/cm^2, respectively, with a 0.8-mg/cm^2 Nb backing facing the beam. Projectile-like reaction fragments in the Xe region were identified with the magnetic mass spectrometer PRISMA placed at the grazing angle of $\theta_{\text{lab}} = 50°$. The measured quantities allowed unequivocal determination of the atomic and mass numbers and the velocity vector for the individual lighter reaction products. A 40×60 mm^2 microchannel plate detector DANTE (Detector
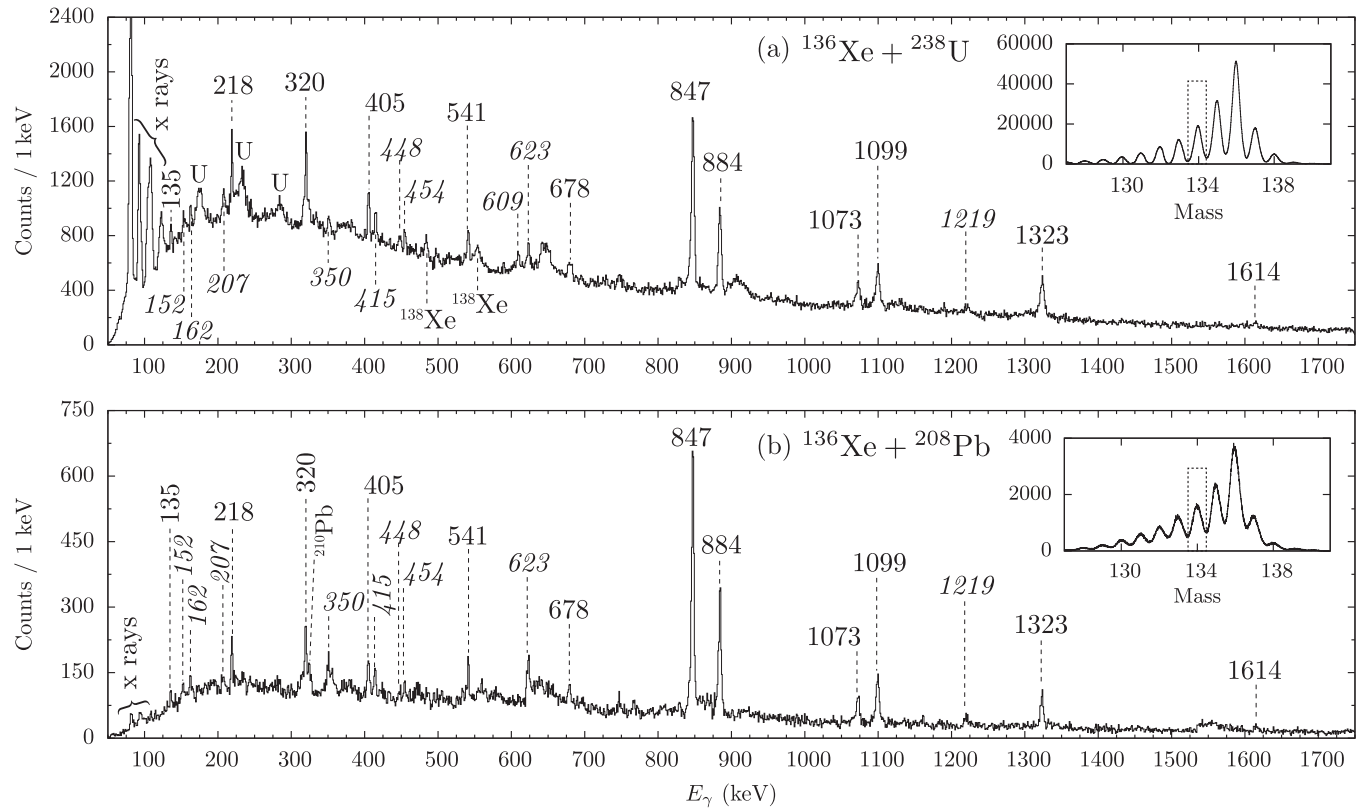
FIG. 1. Doppler-corrected γ-ray spectra gated on ^{134}Xe identified in PRISMA (a) in the ^{136}Xe + ^{238}U experiment and (b) in the ^{136}Xe + ^{208}Pb experiment with indicated γ-ray energies in keV. The spectra are obtained with a cut on the prompt time peak between AGATA and PRISMA. Remaining contaminations of the U and Pb binary reaction partners are marked in the spectra. Italic numbers label newly observed γ-ray transitions.

Array for Multinucleon Transfer Ejectiles) [31,32] covered the angular range which corresponds to the grazing angle for the targetlike reaction product in order to request a kinematic coincidence between the different reaction products. γ rays from excited states in both beam- and targetlike nuclei were detected with the AGATA array [25] in the demonstrator configuration [31] placed 23.5 cm from the target position. The array consisted of 15 large-volume electronically segmented high-purity Ge (HPGe) detectors in five triple cryostats [33]. An event registered by the PRISMA focal-plane detector in coincidence with an AGATA event was taken as a trigger for the data acquisition. Pulse-shape analysis of the fully digitized detector signals was applied to determine the individual interaction points. This information is used by the Orsay forward-tracking algorithm [34] to reconstruct the individual emitted γ-ray energies and determine the first interaction point of the γ ray in the germanium and, thus, the emission angle. Combining this information with the kinematic information of PRISMA, a precise Doppler correction for beam- and targetlike nuclei was performed. Details and results of the analysis procedure are reported in Refs. [35,36].

The Xe Doppler-corrected singles γ-ray spectrum of ^{134}Xe is shown in Fig. 1(a). The corresponding mass spectrum of the Xe isotopes is depicted in the inset. Random background is significantly suppressed by gating on the prompt time-difference peak between AGATA and PRISMA. The full

width at half maximum (FWHM) of the prompt coincidence peak is approximately 16 ns for identified beamlike particles. Transitions belonging to both primary binary partners are present in the γ-ray spectra. Results on the heavy binary partner ^{240}U are presented in Ref. [37].

The ground-state band of ^{134}Xe is visible up to the 6_1^+ state at an excitation energy of 2272.0 keV. The corresponding $6_1^+ \rightarrow 4_1^+$, $4_1^+ \rightarrow 2_1^+$, and $2_1^+ \rightarrow 0_1^+$ decays at 405, 884, and 847 keV, respectively, can be seen in the singles spectrum. Furthermore, a peak at 1073 keV can be identified as the $3^+ \rightarrow 2_1^+$ transition, de-exciting the 1920-keV level. A smaller peak at 1614 keV was reported as the decay of the 2_2^+ state to the stable ground state [24]. Transitions with energies of 135, 162, 541, and 678 keV were already observed in studies of the β decay of ^{134}I [18].

As reported in Ref. [23], we also unambiguously identify the 218-, 320-, 1099-, and 1323-keV γ rays to be transitions of ^{134}Xe. However, the peak intensities in our experiment exceed the previous work by three orders of magnitude. The broad peak at 320 keV in the singles spectrum consists of two peaks with energies of 320 and 323 keV. New peaks well above the background level are observed at 152, 207, 350, 415, 448, 454, 623, and 1219 keV. Peaks at 207, 415, and 448 keV were also visible in the γ-ray spectrum by Shrivastava *et al.*, but were neither marked nor listed as transitions belonging to ^{134}Xe. However, transitions with energies of 152 and 350 keV were
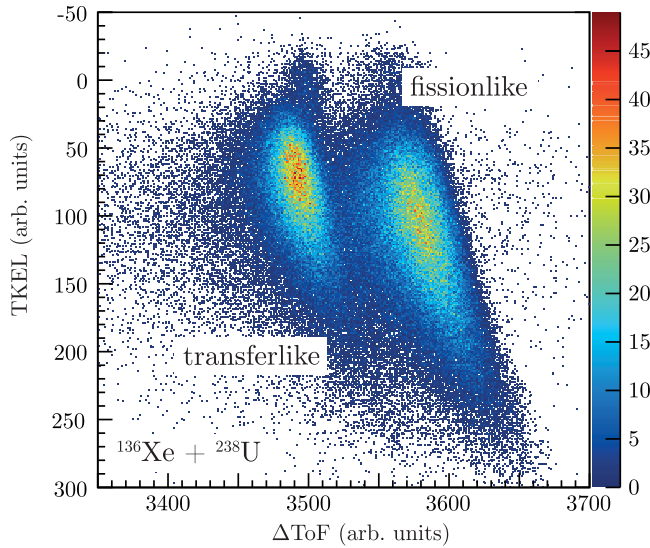
FIG. 2. Matrix of the time difference ΔToF between PRISMA and DANTE plotted against the total kinetic energy loss for ^{134}Xe events in the ^{136}Xe + ^{238}U experiment. Transfer and fission are clearly separated. Note that for the fission channel, the computed TKEL is only qualitative since a binary reaction is assumed.

previously reported and tentatively assigned to low-spin states in an preliminary published level scheme of a ^{nat}Xe$(n,n'\gamma)$ experiment [38].

The ^{136}Xe + ^{238}U experiment allows to distinguish the two production modes of ^{134}Xe, which is populated both as a

fission fragment and as a two-neutron transfer product via particle-particle coincidences. The population of ^{134}Xe in the multinucleon transfer is observed with a cross section of ~70 mb [35]. Simultaneously, ^{134}Xe is populated as a highly excited actinide fission fragment of the ^{238}U$(^{136}$Xe$,F\gamma)$ reaction. In this way, the separation between highly excited fission fragments and preferentially colder transfer products gives valuable additional information related to the population modes of excited states in the identified ejectile nuclei and their level scheme.

In the ^{136}Xe + ^{238}U experiment the fast anode signals of the entrance detector of PRISMA and the DANTE MCP enabled the measurement of time-of-flight differences (ΔToF) between different coincident reaction products entering the PRISMA spectrometer. A significant time difference is observed due to the different kinetic energies and velocities of the fission products compared to the transfer products. The simultaneous measurement of both the momentum and the angle of the beamlike recoils with PRISMA enables a reconstruction of the total kinetic energy loss (TKEL) value of the reaction [39]. As presented in Fig. 2, transferlike and fissionlike fragments are separated as two different domains in a matrix of ΔToF plotted against the TKEL for ejectiles identified as Xe. The computed TKEL value for the fission fragment is not complete and correct since the TKEL calculation is based on the binary-partner reaction system.

The ejectile Doppler-corrected γ-ray spectrum is shown in Fig. 3(a) for transferlike events while γ rays originating from ^{134}Xe fission fragments are sorted into Fig. 3(b). The ground-state $2_1^+ \rightarrow 0_1^+$ transition at 847 keV and the $4_1^+ \rightarrow 2_1^+$
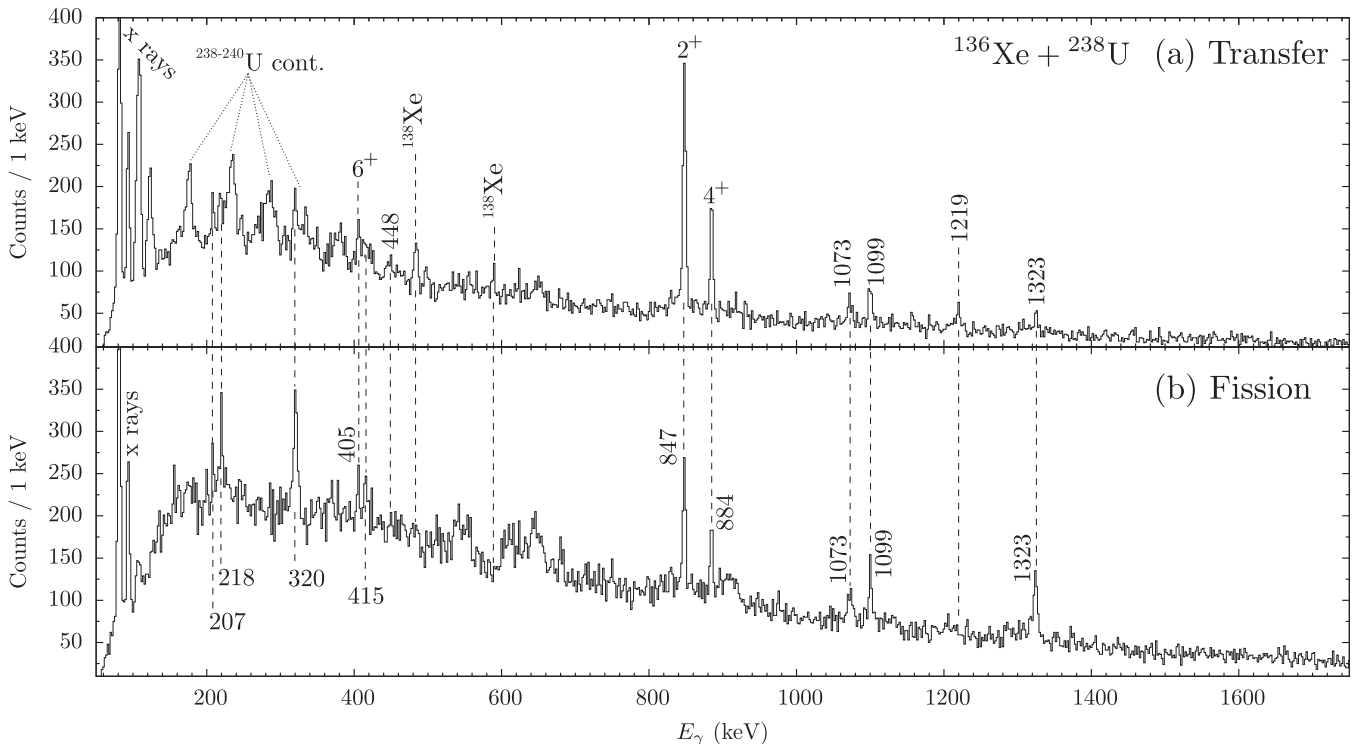

FIG. 3. Doppler-corrected ^{134}Xe γ-ray spectra from the ^{136}Xe + ^{238}U experiment with (a) a gate on transferlike events and (b) events originating from actinide fission.

transition at 884 keV are visible in both spectra, but dominate in the transferlike spectrum. In the transfer case the integral of the 847-keV peak is ten times larger than the integral of the 1323-keV line. For the fission case this factor is reduced to $\sim$1.4. The fission spectrum shows prominent peaks from 207-, 218-, 320-, 415-, and 1323-keV transitions, which are clearly suppressed in the transfer spectrum. Hence, those decaying states are mainly populated in highly excited fission residues. The peak at 1099 keV is visible in both transfer- and fissionlike spectra. In contrast, the 448- and 1219-keV transitions prevail in the transferlike spectrum.

By exploiting the position sensitivity for γ-ray interaction points in AGATA and for ejectile nuclei in the PRISMA entrance detector, it is possible to investigate γ-ray angular distributions of the measured γ rays with respect to the momentum of ^{134}Xe nuclei. In this way, the multipolarities of observed γ-ray transitions are compared and constrained in comparison with well-known and documented γ-ray decays.

The spin alignment is perpendicular to the reaction plane and defined by the magnetic spectrometer itself. In contrast to fusion-evaporation reactions, the spin alignment after multinucleon-transfer reactions is reduced, yet it is large enough to perform detailed angular distributions [40]. However, multinucleon-transfer shows an asymmetry of the spin alignment with respect to the azimuthal angle [41]. Contrarily to traditional detector arrays with single detectors, the AGATA demonstrator can be considered as an extended and continuous HPGe detector. Examples of such continuous distributions are given in Ref. [42]. For each γ ray the first interaction point within AGATA and the reconstructed momentum vector by PRISMA are used to calculate the corresponding angles $\theta_{\gamma,\mathrm{Xe}}$ between the ejectile fragments and the emitted γ rays. The isotropic angular distributions of 1408-keV γ rays from a ^{152}Eu source placed at the target position serve as a geometrical efficiency correction for the detector setup. Moreover, background contributions are carefully selected and subsequently subtracted from the measured angular distributions. The degree of spin orientation with respect to the beam axis strongly depends on the initial formation process and the reaction mechanism. Thus, the angular distributions yield qualitative and tentative results on the γ-ray multipolarities.

The five AGATA triple cluster detectors were placed at backward angles with respect to the PRISMA entrance window. Figure 4 shows the ratio $W(\theta_{\gamma,\mathrm{Xe}})$ between the number of counts in the angular range from 161° to 180° over the number of counts in the 150° to 161° angular range for various strong transitions of known multipolarity ℓ in ^{134,135,136,138}Xe. The horizontal dashed line depicts the mean value $\overline{W}_{\ell=2}$ of the measured ratios for evaluated $E2, \ell = 2$ transitions [24,43–45] that are also labeled in the figure. As anticipated, the 1073-keV $3^+ \rightarrow 2_1^+$ $M1 + E2$ transition in ^{134}Xe with a mixing ratio of $\delta = +0.16(2)$ [24] exhibits a considerable deviation from the mean $\ell = 2$ value. Similarly, $W(\theta_{\gamma,\mathrm{Xe}})$ of the 320-keV transition in ^{134}Xe is more than 2σ off with respect to $\overline{W}_{\ell=2}$, corroborating the assumption that this transition is of $\ell = 1$ dipole character. The angular-distribution ratio of the 1323-keV transition is consistent with an $E2$ multipolarity of $\ell = 2$.
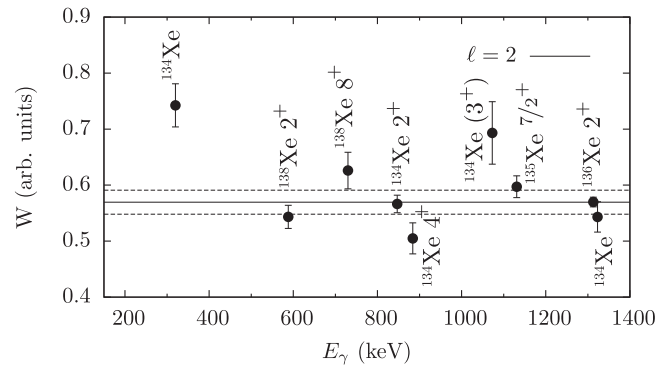

FIG. 4. Ratio $W(\theta_{\gamma,\mathrm{Xe}})$ from γ-ray angular distributions between the number of counts in the angular range from 161° to 180° over the number of counts in the 150° to 161° angular range, measured with AGATA in the ^{136}Xe $+ ^{238}$U experiment for various transitions in Xe isotopes (see labels). The horizontal line depicts the weighted mean ratio for evaluated $I \rightarrow I - 2$ transitions. Dashed lines mark the corresponding standard deviation.

Events with γ-ray multiplicities $M_\gamma \geqslant 2$ are sorted into a $\gamma\gamma$-coincidence matrix. Coincidence spectra are created by projecting the matrix onto one of its axes. A corresponding gate on the 1323-keV peak is shown in Fig. 5; it demonstrates that the 1323-keV transition is coincident with the 218-, 320-, and 207-keV γ rays. Extended results on an improved $\gamma\gamma$-coincidence analysis are the subject of the paragraph related to the ^{136}Xe $+ ^{198}$Pt experiment.

To summarize, the ^{136}Xe $+ ^{238}$U experiment yields results on two different population paths, multinucleon transfer and fission. By means of particle identification, several previously reported transitions as well as new transitions are unambiguously assigned to ^{134}Xe. In the fission-gated γ-ray spectra, six transitions are enhanced with respect to the transfer-gated spectra, suggesting that states with larger excitation energies as well as higher angular momentum are populated.

B. ^{136}Xe $+ ^{208}$Pb

In this experiment, a ^{136}Xe beam provided by the PIAVE+ALPI accelerator complex at an energy of 930 MeV impinged onto a 1 mg/cm^2 thick ^{208}Pb target. PRISMA was placed at the grazing angle of $\theta_{\mathrm{lab}} = 42^\circ$. γ rays were measured
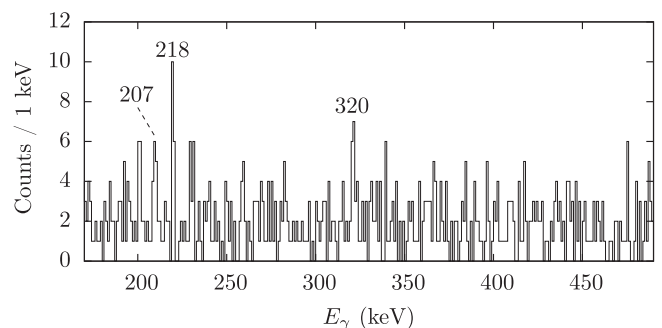

FIG. 5. $\gamma\gamma$-coincidence spectrum of the ^{136}Xe $+ ^{238}$U experiment with a gate around $E_\gamma = 1323$ keV (shown in the inset panel).

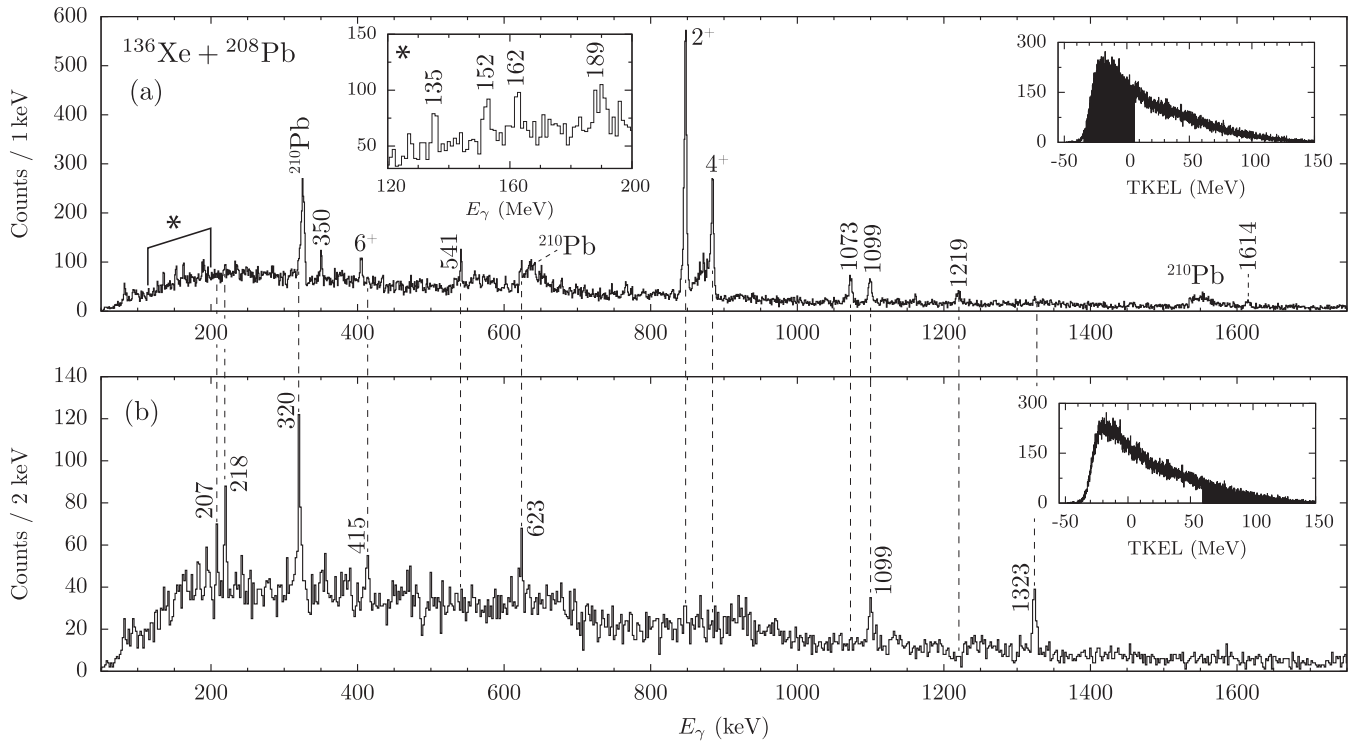FIG. 6. Doppler-corrected ^{134}Xe γ-ray spectra with gates on low and large TKEL values from the ^{136}Xe + ^{208}Pb experiment: (a) gate on low TKEL and (b) gate on large TKEL corresponding to higher excitation energies after the deep-inelastic MNT reaction. The applied gates on the TKEL distributions are shown in the insets. Both spectra are obtained with a cut on the prompt time peak between AGATA and PRISMA.

by the AGATA demonstrator in an earlier configuration in which only three triple clusters were available. The experimental configuration, trigger conditions, as well as the data analysis resemble those described in Sec. II A. The singles γ-ray spectrum depicted in Fig. 1(b) exhibits the same lines as in the ^{136}Xe + ^{238}U experiment, yet there is much less random background from fission present in the spectrum. Further details of the analysis are presented in Refs. [46,47].

Multinucleon transfer reactions populate excitation energies and spins differing substantially from the ones reached by fusion-evaporation reactions or fission residues [27,48]. The total excitation energy can be restricted by gating on the TKEL, which was calculated in a similar way to that described in Sec. II A. In particular, events with small TKEL values are related to reaction products with a lower excitation energy. We remind the reader that as the TKEL is shared between the two reaction products, the excitation energy of both light and heavy reaction products is included in the TKEL distribution. Due to the presence of the two long-lived isomers in the level scheme of ^{134}Xe, the TKEL-gated prompt in-beam γ-ray spectra are excellent tools to discriminate between γ-ray transitions below and above the isomeric states. Thus, TKEL spectra are correlated with coincident γ rays of AGATA. By gating on different TKEL regions, γ-ray transitions between states with different excitation energies and angular momenta can be suppressed or enhanced [27,28]. Figure 6 shows γ-ray spectra for ^{134}Xe obtained with different conditions on the TKEL. The TKEL spectra are presented in the top right insets.

By gating on the low-TKEL region (a), the three lowest $6_1^+ \rightarrow 4_1^+$, $4_1^+ \rightarrow 2_1^+$, and $2_1^+ \rightarrow 0_1^+$ yrast transitions are clearly enhanced in the spectrum. As expected, the 1073-keV transition connecting the low-lying 1920-keV 3^+ state with the 2_1^+ state is only visible in panel (a). Transitions of other low-lying non-yrast states such as the $(5^+) \rightarrow 4_1^+$ at 541 keV, the $(5^+) \rightarrow 6_1^+$ at 135 keV γ rays, and a new peak at 1219 keV are visible as well. The gate also reveals transitions with a small branching ratio such as the 189 keV γ ray connecting the 1920 keV 3^+ state with the 4_1^+ yrast state. All these lower-energy transitions, including the yrast γ-ray transitions below the 10^+ isomer vanish for gates on large TKEL values in Fig. 6(b). The peaks at 207, 218, 415, 623, and 1323 keV and a broad peak at 320 keV only appear at large TKEL. The 1099-keV line is visible for both TKEL domains in Fig. 6. In conclusion, due to the presence of two long-lived isomers, gates on large TKEL can indeed entirely suppress de-excitations of states below the isomeric states. Hence, there is strong evidence that the above-mentioned transitions (207, 218, 320, 415, 623, and 1323 keV) are in fact located at higher excitation energies in the level scheme. The singles spectra of both AGATA experiments exhibit a high-statistics peak at 1099 keV.

C. ^{136}Xe + ^{198}Pt

In this experiment, a 850-MeV ^{136}Xe beam provided by the 88-inch cyclotron at LBNL impinged onto a 92% isotopically enriched self-supporting 420-μg/cm^2 ^{198}Pt target. γ rays were detected by the GAMMASPHERE array, which consisted of 103 Compton-suppressed HPGe detectors in this experiment [29]. Both polar and azimuthal angles and the time-of-flight difference ΔToF between the detection of
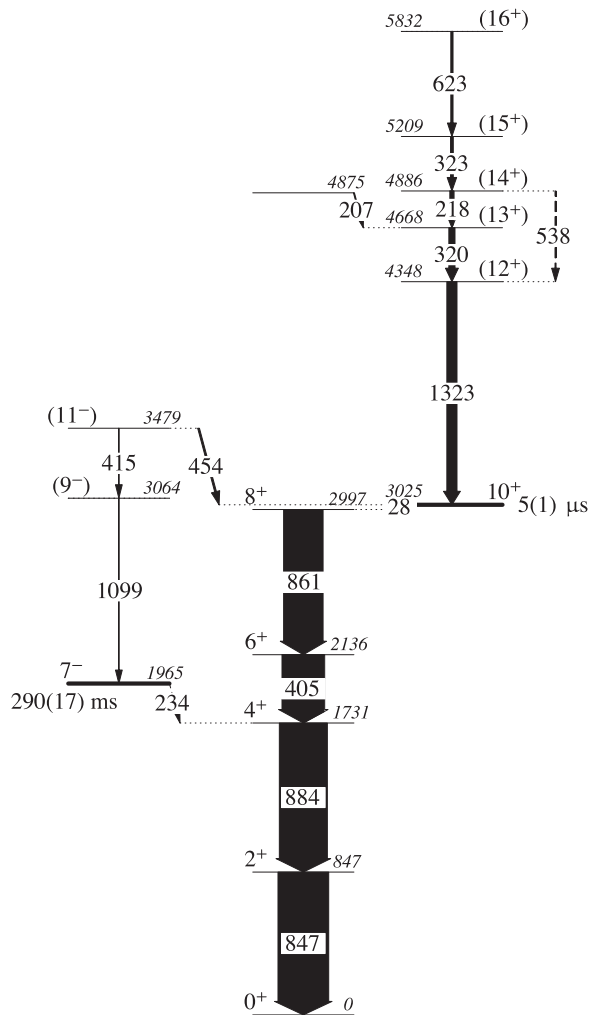
FIG. 7. Partial experimental level scheme of ^{134}Xe with the newly observed γ-ray transitions above the 10^+ and 7^- isomers. Intensities of the yrast cascade below the isomer are extracted from the out-of-beam delayed $\gamma\gamma$ matrix and normalized to the 2_1^+ decay; intensities above the isomer are extracted from the prompt matrix and normalized to the intensity of the 1323-keV transition. The intensity balance between the ground-state sequence and the high-spin states is extracted from the ^{136}Xe $+$ ^{208}Pb dataset.

beamlike and targetlike reaction products were measured with the gas-filled parallel-plate avalanche chamber ancillary detector CHICO (Compact Heavy Ion Counter) [30], thus allowing for an event-by-event Doppler shift correction for emitted γ rays. Detailed descriptions of the channel selection and data analysis are given in Ref. [3].

The experimental data were sorted into three two-dimensional matrices gated on beamlike fragments: (i) an in-beam Doppler-corrected prompt $\gamma\gamma$ matrix, (ii) an out-of-beam delayed-delayed $\gamma\gamma$ matrix, and (iii) a delayed-prompt $\gamma\gamma$ matrix. The time window for the delayed γ rays was 45 to 780 ns. Matrix (i) enables the identification of prompt transitions which feed the long-lived 5-μs 10^+ isomer at 3025 keV.

Spins and parities have been established for levels in ^{134}Xe up to the 10^+ state at 3025 keV [24] (see level scheme in
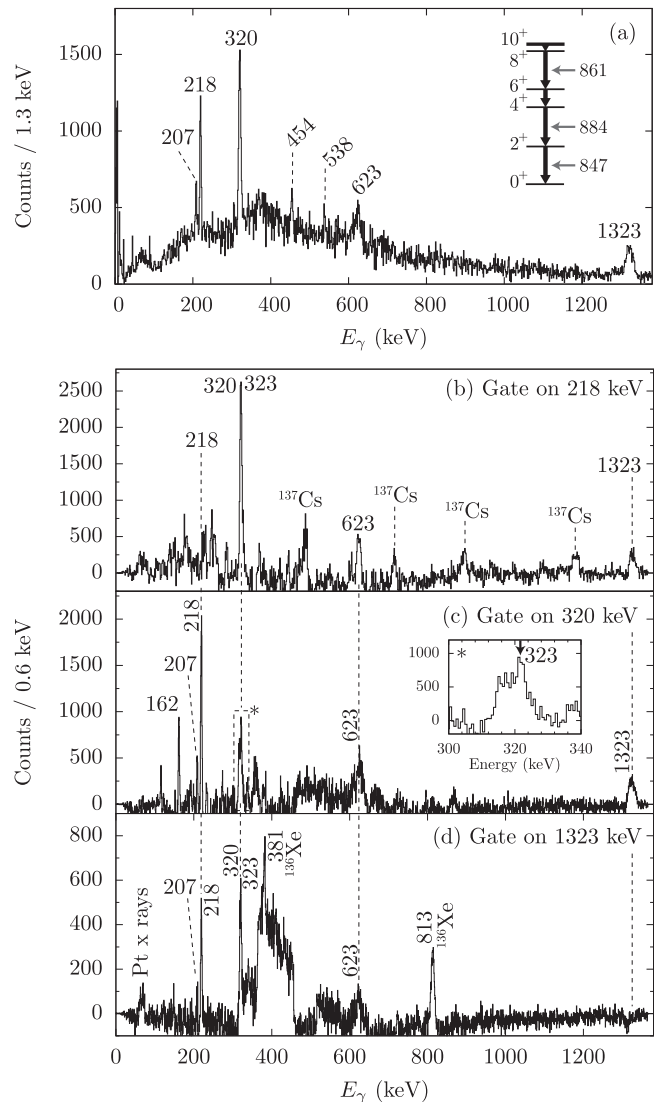

FIG. 8. (a) Sum of GAMMASHERE delayed-prompt $\gamma\gamma$-coincidence spectra with gates on the delayed 847-keV $2_1^+ \rightarrow 0_1^+$, 884-keV $4_1^+ \rightarrow 2_1^+$, and 861-keV $8_1^+ \rightarrow 6_1^+$ yrast transitions (as indicated in the inset miniature levelscheme). (b) to (d): Prompt $\gamma\gamma$-coincidence spectra with gates on 218, 320, and 1323 keV. A closeup of the energy region around 320 keV is shown in the inset in panel (c).

Fig. 7). The 10^+ isomer decays via 28- and 861-keV γ rays to the 8_1^+ and 6_1^+ states. Due to electron conversion, the 28-keV transition is not observable in either one of the experiments, yet the 861-keV γ-ray decay is visible by gating on the transitions of the 4_1^+ and the 2_1^+ yrast states at 847 and 884 keV in the ^{136}Xe $+$ ^{198}Pt out-of-beam delayed $\gamma\gamma$ matrix, respectively. A sum of gates on the delayed 847-, 884-, and 861-keV γ rays in the prompt-delayed matrix in Fig. 8(a) yields prompt coincidence peaks at 207, 218, 320, 454, 538, 623, and 1323 keV. Therefore, these transitions are located above the 10^+ state feeding the isomer.

Background-subtracted prompt $\gamma\gamma$-coincidence spectra with gates on 218, 320, and 1323 keV are shown in Figs. 8(b)–8(d). The 1323-keV transition is mutually coincident with

the 218- and 320-keV γ rays, verifying these transitions to be members of a cascade above the 10^+ isomer. In this measurement the 1323-keV gate exhibits contamination due to the nearby 1313-keV $2^+ \rightarrow 0^+$ transition in ^{136}Xe. A broad accumulation of counts around 400 keV is subsequently caused by falsely Doppler-corrected targetlike ^{198}Pt γ rays. The 6.3(1)-keV FWHM of the 320-keV peak is broader than that of the neighboring peaks (e.g., FWHM$_{218\,\text{keV}}$ = 3.54(9) keV). A gate on the left part of the 320-keV peak reveals a second peak at 323 keV, as depicted in Fig 8(c). Coincidences with 623-keV γ rays are present in all gated spectra; a coincidence with the 207-keV line is observed except for the 218-keV gate.

The construction of the level scheme which is built on top of the 10^+ isomeric state is based on the prompt $\gamma\gamma$ coincidences and the efficiency-corrected γ-ray intensities from the GAMMASPHERE experiment. The extended and modified level scheme is presented in Fig. 7. Intensities of the yrast cascade below the isomer are extracted from the out-of-beam delayed $\gamma\gamma$ matrix and normalized to the 2_1^+ decay; intensities above the isomer are normalized to the intensity of the 1323-keV transition. The intensity balance between the ground-state sequence and the high-spin structure is extracted from the ^{136}Xe + ^{208}Pb dataset.

The intensity relations affirm the placement of the 1323-keV transition on top of the isomer, fed by the 320- and 218-keV transitions. Fotiades *et al.* reported two more lines to be in coincidence with the 1323-keV line: 323 and 541 keV [22]. The intensity of the 323-keV line corroborates a placement directly above the 4886-keV state. The 541-keV transition expected to be in coincidence with the 320- and the 1323-keV transition is neither observed in the prompt spectra nor in the large-TKEL gated AGATA data. The 541-keV line visible in the low-TKEL gated γ-ray spectrum in Fig. 6(a) can be attributed to the low-spin structure below the isomer [24]. However, a line at 538 keV is visible in the delayed-prompt coincidence spectrum in Fig. 8(a) and, consequently, it is part of a cascade above the isomer. Indeed, the sum of the 320- and 218-keV transitions suggests that the transition of 538 keV bypasses the 320- and 218-keV γ rays. The 623-keV transition is coincident with all transitions of the cascade and, thus,

placed on top of the 5209-keV state based on its low intensity. The line at 207 keV coincides with the 320- and 1323-keV γ rays, but not with the 218-keV transition or other decays from higher-lying states. It is assumed to feed the 4668-keV state.

Shrivastava *et al.* tentatively assigned a 1100-keV line to be a $(9^-) \rightarrow 7^-$ transition feeding the 290-ms $E_x = 1965$ keV 7^- isomer [23]. This assignment was based on a comparison with results of a LSSM calculation. A 1100-keV transition was also found to connect the mixed-symmetry 2_3^+ state with the 2_1^+ yrast state in a later experiment [21]. As shown in Sec. II B, the 1099-keV transition appears in both TKEL-gated γ-ray spectra of the ^{136}Xe + ^{208}Pb experiment in Fig. 6. Consequently, it is interpreted as a doublet. The gate on low TKEL in the ^{136}Xe + ^{208}Pb experiment predominantly selects the $2_3^+ \rightarrow 2_1^+$ transition. On the other hand, the decay of the 2_1^+ state to the ground state is not present in the γ-ray spectrum gated on large TKEL. Subsequently, the 1099-keV transition visible in Fig. 6(b) is not connected to the yrast band and has to be placed on top of an isomeric state. Due to missing coincidences with any known or newly observed transitions above the 10^+ isomer, it is placed on top of the second isomer feeding directly the 7^- isomer at 1965 keV. A 612-keV $(11^-) \rightarrow (9^-)$ transition, which was suggested in Ref. [23] to sit on top of the 1099-keV transition is not observed in either AGATA or GAMMASPHERE spectra. It was shown before that the 415-keV γ ray was found in the ^{136}Xe + ^{238}U fission γ-ray spectrum as well as in the γ-ray spectrum of the ^{136}Xe + ^{238}U experiment gated on large TKEL. Since the 415-keV transition is also not observed in coincidence with any transitions above the 10^+ isomer, the transition is placed above the long-lived 7^- isomer feeding the 3064-keV state. The newly found 454-keV transition also does not show any γ-ray coincidences with members of the band above the 10^+ isomer. The 454-keV transition is placed directly above the 10^+ isomer decaying from the (already introduced) excited (11^-) state at 3479 keV into the 10^+ isomer. The energy differences between the 3479-keV state and the 3025-keV 10^+ state match nicely. In this way, a decay branch connects the negative-parity states above the 7^- isomer with the 10^+ excited state. The 448-keV transition present in the AGATA

TABLE I. Energies, assignments, and relative in-beam intensities for transitions observed in ^{134}Xe above the 10^+ and 7^- isomers. The energies are fitted in the AGATA datasets; intensities are taken from the GAMMASPHERE measurement. The uncertainties in the transition energies are ± 0.5 keV. Possible spin-parity assignments are discussed in Sec. III.

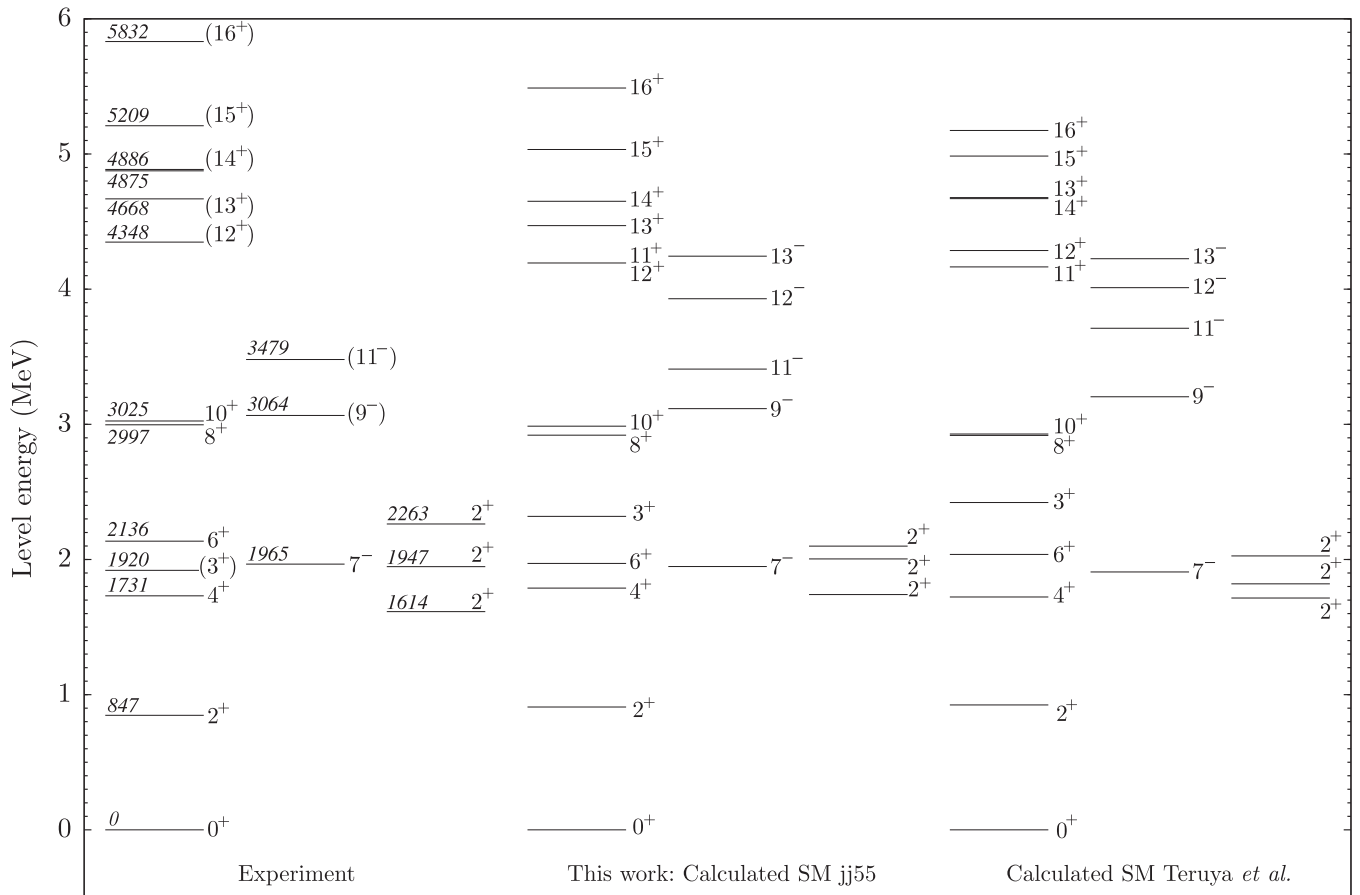| E_γ (keV)	E_i	E_f	I_i^π	I_f^π	I_γ
		Transitions feeding the 10^+ isomer			
207	4875	4668		(13^+)	2.3(2)
218	4886	5290	(14^+)	(13^+)	10.4(2)
320	4668	4348	(13^+)	(12^+)	16.1(25)
323	5209	4886	(15^+)	(14^+)	7.2(24)
454	3479	3025	(11^-)	10^+	4.7(3)
538	5209	4668	(14^+)	(12^+)	2.7(3)
623	5290	4668	(16^+)	(15^+)	5.9(2)
1323	4348	3025	(12^+)	10^+	27.6(7)
		Transitions feeding the 7^- isomer			
415	3479	3064	(11^-)	(9^-)	
1099	3064	1965	(9^+)	7^-	

FIG. 9. Comparison of the experimental energy spectra (left panel) with the results of the shell-model calculations within the jj55 effective interaction (middle panel) and by Teruya *et al.* [51] (right panel). Note that in all panels the states are separated into three columns for the positive-parity, negative-parity, and higher-lying 2^+ states.

spectra is not visible in any coincidence spectra and could not be included in the level scheme. The γ-ray transitions above the isomeric states and their corresponding intensities are summarized in Table I. Possible spin-parity assignments are discussed in Sec. III. In brief, the ^{136}Xe + ^{198}Pt data yields crucial results on the extended and revised level structure above the two isomers by exploiting delayed-prompt and prompt $\gamma\gamma$ coincidences.

III. SHELL MODEL CALCULATION

The extended level scheme was compared to results of two different shell-model calculations for ^{134}Xe. The first calculations were carried out in the proton-neutron formalism without any truncations for positive- and negative-parity states in the full $gdsh$ valence space outside the ^{100}Sn core between the magic numbers 50 and 82, including the $0g_{7/2}, 1d_{5/2}, 1d_{3/2}, 2s_{1/2}$, and $0h_{11/2}$ orbitals for both protons and neutrons. The shell-model code NUSHELLX@MSU [11] was employed using the jj55 effective interaction obtained by Brown *et al.* [49] based on a renormalized G matrix derived from the CD-Bonn nucleon-nucleon interaction [50] considering ^{132}Sn as the core nucleus.

An independent extensive theoretical study of nuclei around mass 130 was published by Teruya *et al.* [51]. The

results include excited states and electromagnetic transition probabilities for Xe isotopes within the shell model in the $gdsh$ model space including the $0g_{7/2}, 1d_{5/2}, 1d_{3/2}, 2s_{1/2}$, and $0h_{11/2}$ orbitals. The effective interaction consists of spherical single-particle energies and phenomenological two-body effective interactions consisting of monopole-pairing, quadrupole-pairing, and quadrupole-quadrupole terms. Further newly introduced higher-order pairing interactions are also taken into account. Single-particle energies (SPE) were adopted from the experimental excited states of ^{133}Sb (proton SPEs) and ^{131}Sn (neutron SPEs) [51].

In Fig. 9 the results of both shell-model calculations (middle and right panels) have been compared to the experimental levels (left panel). Note that in all panels the states are separated into three columns for (i) positive-parity and (ii) negative-parity states visible in the experiments from this work and (iii) $2^+_{2,3,4}$ states from the literature as a further benchmark for the validity of the shell-model calculations. Good agreement is obtained for the even-spin states of the yrast band up to spin 10^+. In particular, both calculations reproduce the small energy spacing between the 8^+ and the 10^+ state. Only the 3^+_1 state with a $61\% \pi g^3_{7/2} d^1_{5/2}$ configuration is placed in both theoretical results too high in energy above the 6^+_1 state with respect to the experimentally obtained sequence. The spin of the (3^+_1) state was only assigned tentatively in the

literature [18]. The position of the experimental 7^- isomer state with regard to the even-spin yrast cascade is also mirrored with high precision in the calculations. Both calculations reproduce the three low-lying $2^+_{2,3,4}$ states.

Above the 10^+ isomeric state, both shell-model approaches predict 11^+ and 12^+ states more than 1200-keV higher-lying in energy. Within the jj55 interaction, the 12^+ state is located below the 11^+ state with nearly degenerate excitation energy. The 1323-keV γ ray, de-exciting the 4348-keV state, is inferred to be a stretched $E2$ transition (see Sec. II A). This would be a consistent scenario and the two shell-model calculations suggest the 4348-keV state to be tentatively assigned a spin-parity value of 12^+. In the jj55 calculation, states on top of the 12^+ and 11^+ pair are predicted to have positive parity with consecutive spin differences of $\Delta I = 1$, giving the corresponding transitions $M1$ character. This calculation also adequately reproduces the experimental energy spacings of states in the energy range from 4.3 up to 5.8 MeV, besides the yet unresolved 4875-keV state that de-excites via a weak 207-keV γ ray. From this point of view, the states on top of the 4348-keV state up to spin 16^+ are of positive parity, connected by magnetic dipole transitions.

The calculation performed by Teruya *et al.* suggests that the 14^+ state lies, nearly degenerate in energy, below the 13^+ state. According to the tentative (12^+) assignment for the 4348-keV state and the measured multipolarity $\Delta l = 1$ of the feeding 320-keV transition, the spin parity of the 4668-keV state is possibly 13^+.

Moreover, the SM results provide insight into the structure of the isomeric states and the levels built on top. The 10^+ state is calculated to be of $\nu h_{11/2}^{-2}$ character with a configuration of 68% $\nu_{10^+} \otimes \pi_{0^+}$ and 23% $\nu_{10^+} \otimes \pi_{2^+}$ by the jj55 shell-model calculation. Up to spin 16^+, the first high-spin states above the 10^+ state consist of a neutron 10^+ configuration coupled to even-spin proton configurations. The 7^- isomer is dominated by the $\nu d_{3/2}^{-1} h_{11/2}^{-1}$ neutron configuration. According to the calculated level schemes there is strong evidence to interpret the 1099-keV transition, placed above the 7^- isomer, as the decay of the 9^- state. Teruya *et al.* as well as the jj55 calculation describe the negative-parity states above the 7^- isomer with a stretched angular momentum of $7\hbar$ coupled to

the proton quadrupole excited states $(0^+, 2^+, 4^+)$. Further on, a sequence of 12^- and 13^- states is predicted at higher excitation energies.

IV. CONCLUSIONS

In summary, new high-spin states in ^{134}Xe on top of the two long-lived isomers have been discovered. The results are based on γ-ray spectroscopy after MNT reactions and fission fragment spectroscopy. $\gamma\gamma$ coincidence relations, γ-ray angular distributions, and excitation energies from the total kinetic energy loss and fission fragments are used to construct an extended decay scheme including several newly observed states and γ-ray transitions. The high-spin structure above the 10^+ isomer could be unambiguously identified for the first time by delayed-prompt $\gamma\gamma$ coincidences. The extended and revised level scheme of ^{134}Xe is constructed up to an excitation energy of 5.832 MeV with tentative spin-parity assignments up to 16^+. Previous assignments of states above the 7^- isomer, with the exception of the 3064-keV level, have been revised by introducing two newly observed γ rays in two decay branches. Recent shell-model calculations reproduce the experimental findings remarkably well and corroborate most of the suggested assignments.

[1] B. Fogelberg, K. Heyde, and J. Sau, Nucl. Phys. A **352**, 157 (1981).

[2] J. Genevey, J. A. Pinston, C. Foin, M. Rejmund, R. F. Casten, H. Faust, and S. Oberstedt, Phys. Rev. C **63**, 054315 (2001).

[3] J. J. Valiente-Dobón, P. H. Regan, C. Wheldon, C. Y. Wu, N. Yoshinaga, K. Higashiyama, J. F. Smith, D. Cline, R. S. Chakrawarthy, R. Chapman, M. Cromaz, P. Fallon, S. J. Freeman, A. Görgen, W. Gelletly, A. Hayes, H. Hua, S. D. Langdown, I. Y. Lee, X. Liang, A. O. Macchiavelli, C. J. Pearson, Z. Podolyák, G. Sletten, R. Teng, D. Ward, D. D. Warner, and A. D. Yamamoto, Phys. Rev. C **69**, 024316 (2004).

[4] T. Shizuma, Z. G. Gan, K. Ogawa, H. Nakada, M. Oshima, Y. Toh, T. Hayakawa, Y. Hatsukawa, M. Sugawara, Y. Utsuno, and Z. Liu, EPJ A **20**, 207 (2004).

[5] M. Müller-Veggian, Y. Gono, R. M. Lieder, A. Neskakis, and C. Mayer-Böricke, Nucl. Phys. A **304**, 1 (1978).

[6] J. C. Merdinger, F. A. Beck, E. Bozek, T. Byrski, C. Gehringer, Y. Schutz, and J. P. Vivien, Nucl. Phys. A **346**, 281 (1980).

[7] M. Ferraton, R. Bourgain, C. M. Petrache, D. Verney, F. Ibrahim, N. de Séréville, S. Franchoo, M. Lebois, C. Phan Viet, L. Sagui, I. Stefan, J. Clavelin, and M. Vilmay, EPJ A **35**, 167 (2008).

[8] M. Lach, J. Styczen, R. Julin, M. Piiparinen, H. Beuscher, P. Kleinheinz, and J. Blomqvist, Z. Phys. A **319**, 235 (1984).

[9] E. Caurier, G. Martínez-Pinedo, F. Nowacki, A. Poves, J. Retamosa, and A. P. Zuker, Phys. Rev. C **59**, 2033 (1999).

[10] E. Caurier and G. Martínez-Pinedo, Nucl. Phys. A **704**, 60 (2002).

[11] B. A. Brown and W. D. M. Rae, Nucl. Data Sheets **120**, 115 (2014).

[12] K. Higashiyama and N. Yoshinaga, Phys. Rev. C **83**, 034321 (2011).

[13] K. Sieja, G. Martínez-Pinedo, L. Coquard, and N. Pietralla, Phys. Rev. C **80**, 054311 (2009).

[14] K. Higashiyama, N. Yoshinaga, and K. Tanabe, Phys. Rev. C **65**, 054317 (2002).

[15] W. G. Winn and D. G. Sarantites, Phys. Rev. **184**, 1188 (1969).

[16] E. Achterberg, E. Y. de Aisenberg, F. C. Iglesias, A. E. Jech, J. A. Moragues, D. Otero, M. L. Pérez, A. N. Proto, J. J. Rossi, W. Scheuer, and J. F. Suárez, Phys. Rev. C **4**, 188 (1971).

[17] C. D. Coryell, H. N. Erten, P. K. Hopke, W. B. Walters, R. Dams, and H. C. Griffin, Nucl. Phys. A **179**, 689 (1972).

[18] J. M. Gualda, R. N. Saxena, and F. C. Zawislak, Nucl. Phys. A **234**, 357 (1974).

[19] G. Jakob, N. Benczer-Koller, G. Kumbartzki, J. Holden, T. J. Mertzimekis, K.-H. Speidel, R. Ernst, A. E. Stuchbery, A. Pakou, P. Maier-Komor, A. Macchiavelli, M. McMahan, L. Phair, and I. Y. Lee, Phys. Rev. C **65**, 024316 (2002).

[20] K. H. Speidel, H. Busch, S. Kremeyer, U. Knopp, J. Cub, M. Bussas, W. Karle, K. Freitag, U. Grabowy, and J. Gerber, Nucl. Phys. A **552**, 140 (1993).

[21] T. Ahn, L. Coquard, N. Pietralla, G. Rainovski, A. Costin, R. V. F. Janssens, C. J. Lister, M. Carpenter, S. Zhu, and K. Heyde, Phys. Lett. B **679**, 19 (2009).

[22] N. Fotiades, R. O. Nelson, M. Devlin, J. A. Cizewski, J. A. Becker, W. Younes, R. Krücken, R. M. Clark, P. Fallon, I. Y. Lee, A. O. Macchiavelli, T. Ethvignot, and T. Granier, Phys. Rev. C **75**, 054322 (2007).

[23] A. Shrivastava, M. Caamaño, M. Rejmund, A. Navin, F. Rejmund, K. H. Schmidt, A. Lemasson, C. Schmitt, L. Gaudefroy, K. Sieja, L. Audouin, C. O. Bacri, G. Barreau, J. Benlliure, E. Casarejos, X. Derkx, B. Fernández-Domínguez, C. Golabek, B. Jurado, T. Roger, and J. Taieb, Phys. Rev. C **80**, 051305 (2009).

[24] A. A. Sonzogni, Nucl. Data Sheets **103**, 1 (2004).

[25] S. Akkoyun *et al.*, Nucl. Instr. Meth. Phys. Res. A **668**, 26 (2012).

[26] A. Stefanini, L. Corradi, G. Maron, A. Pisent, M. Trotta, A. Vinodkumar, S. Beghini, G. Montagnoli, F. Scarlassara, G. Segato, A. D. Rosa, G. Inglima, D. Pierroutsakou, M. Romoli, M. Sandoli, G. Pollarolo, and A. Latina, Nucl. Phys. A **701**, 217 (2002).

[27] S. Szilner, C. A. Ur, L. Corradi, N. Marginean, G. Pollarolo, A. M. Stefanini, S. Beghini, B. R. Behera, E. Fioretto, A. Gadea, B. Guiot, A. Latina, P. Mason, G. Montagnoli, F. Scarlassara, M. Trotta, G. de Angelis, F. Della Vedova, E. Farnea, F. Haas, S. Lenzi, S. Lunardi, R. Marginean, R. Menegazzo, D. R. Napoli, M. Nespolo, I. V. Pokrovsky, F. Recchia, M. Romoli, M.-D. Salsac, N. Soić, and J. J. Valiente-Dobón, Phys. Rev. C **76**, 024604 (2007).

[28] L. Corradi, S. Szilner, G. Pollarolo, D. Montanari, E. Fioretto, A. Stefanini, J. Valiente-Dobón, E. Farnea, C. Michelagnoli, G. Montagnoli, F. Scarlassara, C. Ur, T. Mijatović, D. J. Malenica, N. Soić, and F. Haas, Nucl. Instr. Meth. Phys. Res. B **317**, 743 (2013).

[29] I.-Y. Lee, Nucl. Phys. A **520**, c641 (1990).

[30] M. W. Simon, D. Cline, C. Y. Wu, R. W. Gray, R. Teng, and C. Long, Nucl. Instr. Methods Phys. Res. Sec. A **452**, 205 (2000).

[31] A. Gadea, E. Farnea, J. J. Valiente-Dobón, B. Million, D. Mengoni, D. Bazzacco, F. Recchia, A. Dewald, T. Pissulla, W.

Rother, G. de Angelis *et al.*, Nucl. Instr. Meth. Phys. Res. A **654**, 88 (2011).

[32] J. J. Valiente-Dobón *et al.*, Acta. Phys. Pol. B **37**, 225 (2006).

[33] A. Wiens, H. Hess, B. Birkenbach, B. Bruyneel, J. Eberth, D. Lersch, G. Pascovici, P. Reiter, and H.-G. Thomas, Nucl. Instr. Meth. Phys. Res. A **618**, 223 (2010).

[34] A. Lopez-Martens, K. Hauschild, A. Korichi, J. Roccaz, and J.-P. Thibaud, Nucl. Instr. Meth. Phys. Res. A **533**, 454 (2004).

[35] A. Vogt, B. Birkenbach, P. Reiter, L. Corradi, T. Mijatović, D. Montanari, S. Szilner, D. Bazzacco, M. Bowry, A. Bracco, B. Bruyneel, F. C. L. Crespi, G. de Angelis, P. Désesquelles, J. Eberth, E. Farnea, E. Fioretto, A. Gadea, K. Geibel, A. Gengelbach, A. Giaz, A. Görgen, A. Gottardo, J. Grebosz, H. Hess, P. R. John, J. Jolie, D. S. Judson, A. Jungclaus, W. Korten, S. Leoni, S. Lunardi, R. Menegazzo, D. Mengoni, C. Michelagnoli, G. Montagnoli, D. Napoli, L. Pellegri, G. Pollarolo, A. Pullia, B. Quintana, F. Radeck, F. Recchia, D. Rosso, E. Şahin, M. D. Salsac, F. Scarlassara, P.-A. Söderström, A. M. Stefanini, T. Steinbach, O. Stezowski, B. Szpak, C. Theisen, C. Ur, J. J. Valiente-Dobón, V. Vandone, and A. Wiens, Phys. Rev. C **92**, 024619 (2015).

[36] B. Birkenbach, Ph.D. thesis, Universität zu Köln, 2014, http://kups.ub.uni-koeln.de/5648/.

[37] B. Birkenbach, A. Vogt, K. Geibel, F. Recchia, P. Reiter, J. J. Valiente-Dobón, D. Bazzacco, M. Bowry, A. Bracco, B. Bruyneel, L. Corradi, F. C. L. Crespi, G. de Angelis, P. Désesquelles, J. Eberth, E. Farnea, E. Fioretto, A. Gadea, A. Gengelbach, A. Giaz, A. Görgen, A. Gottardo, J. Grebosz, H. Hess, P. R. John, J. Jolie, D. S. Judson, A. Jungclaus, W. Korten, S. Lenzi, S. Leoni, S. Lunardi, R. Menegazzo, D. Mengoni, C. Michelagnoli, T. Mijatović, G. Montagnoli, D. Montanari, D. Napoli, L. Pellegri, G. Pollarolo, A. Pullia, B. Quintana, F. Radeck, D. Rosso, E. Şahin, M. D. Salsac, F. Scarlassara, P.-A. Söderström, A. M. Stefanini, T. Steinbach, O. Stezowski, S. Szilner, B. Szpak, C. Theisen, C. Ur, V. Vandone, and A. Wiens, Phys. Rev. C **92**, 044319 (2015).

[38] C. A. McGrath, M. F. Villaniand, D. P. Diprete, P. E. Garrett, M. Yeh, S. W. Yates, and Z. Revay (eds.), *Proceedings of the 9th International Symposium on Capture Gamma-Ray Spectroscopy and Related Topics, Budapest, Hungary, October 1996* (Springer, Budapest, Hungary, 1997), Vol. 1, p. 299.

[39] A. B. Brown, C. W. Snyder, W. A. Fowler, and C. C. Lauritsen, Phys. Rev. **82**, 159 (1951).

[40] P. Aguer, R. P. Schmitt, G. J. Wozniak, D. Habs, R. M. Diamond, C. Ellegaard, D. L. Hillis, C. C. Hsu, G. J. Mathews, L. G. Moretto, G. U. Rattazzi, C. P. Roulet, and F. S. Stephens, Phys. Rev. Lett. **43**, 1778 (1979).

[41] D. Montanari, S. Leoni, D. Mengoni, J. J. Valiente-Dobon, G. Benzoni, N. Blasi, G. Bocchi, P. F. Bortignon, S. Bottoni, A. Bracco, F. Camera, P. Casati, G. Colò, A. Corsi, F. C. L. Crespi, B. Million, R. Nicolini, O. Wieland, D. Bazzacco, E. Farnea, G. Germogli, A. Gottardo, S. M. Lenzi, S. Lunardi, R. Menegazzo, G. Montagnoli, F. Recchia, F. Scarlassara, C. Ur, L. Corradi, G. de Angelis, E. Fioretto, D. R. Napoli, R. Orlandi, E. Sahin, A. M. Stefanini, R. P. Singh, A. Gadea, S. Szilner, M. Kmiecik, A. Maj, W. Meczynski, A. Dewald, T. Pissulla, and G. Pollarolo, Phys. Rev. C **85**, 044301 (2012).

[42] L. Pellegri, A. Bracco, F. Crespi, S. Leoni, F. Camera, E. Lanza, M. Kmiecik, A. Maj, R. Avigo, G. Benzoni, N. Blasi,

C. Boiano, S. Bottoni, S. Brambilla, S. Ceruti, A. Giaz, B. Million, A. Morales, R. Nicolini, V. Vandone, O. Wieland, D. Bazzacco, P. Bednarczyk, M. Bellato, B. Birkenbach, D. Bortolato, B. Cederwall, L. Charles, M. Ciemala, G. D. Angelis, P. Désesquelles, J. Eberth, E. Farnea, A. Gadea, R. Gernhäuser, A. Görgen, A. Gottardo, J. Grebosz, H. Hess, R. Isocrate, J. Jolie, D. Judson, A. Jungclaus, N. Karkour, M. Krzysiek, E. Litvinova, S. Lunardi, K. Mazurek, D. Mengoni, C. Michelagnoli, R. Menegazzo, P. Molini, D. Napoli, A. Pullia, B. Quintana, F. Recchia, P. Reiter, M. Salsac, B. Siebeck, S. Siem, J. Simpson, P.-A. Söderström, O. Stezowski, C. Theisen, C. Ur, J. V. Dobon, and M. Zieblinski, Phys. Lett. B **738**, 519 (2014).

[43] B. Singh, A. Rodionov, and Y. Khazov, Nucl. Data Sheets **109**, 517 (2008).

[44] A. A. Sonzogni, Nucl. Data Sheets **95**, 837 (2002).

[45] A. A. Sonzogni, Nucl. Data Sheets **98**, 515 (2003).

[46] R. Kempley *et al.*, Acta. Phys. Pol. B **42**, 717 (2011).

[47] M. Siciliano *et al.*, LNL Annual Report 2014, **241**, 63, 2015, http://www.lnl.infn.it/˜annrep/read_ar/2014/contributions/pdfs/063_B_127_B122.pdf.

[48] L. Corradi, G. Pollarolo, and S. Szilner, J. Phys. G **36**, 113101 (2009).

[49] B. A. Brown, N. J. Stone, J. R. Stone, I. S. Towner, and M. Hjorth-Jensen, Phys. Rev. C **71**, 044317 (2005).

[50] R. Machleidt, F. Sammarruca, and Y. Song, Phys. Rev. C **53**, R1483 (1996).

[51] E. Teruya, N. Yoshinaga, K. Higashiyama, and A. Odahara, Phys. Rev. C **92**, 034320 (2015).